JOURNAL OF ENVIRONMENTAL SCIENCES 95 (2020) 99–110

Available online at www.sciencedirect.com

ScienceDirect

www.elsevier.com/locate/jes

JES JOURNAL OF ENVIRONMENTAL SCIENCES

www.jesc.ac.cn

Chemical characteristics and sources of water-soluble organic aerosol in southwest suburb of Beijing

Ruolan Hu[1,2,**], *Qingcheng Xu*[1,2,**], *Shuxiao Wang*[1,2,*], *Yang Hua*[1,2], *Noshan Bhattarai*[1,2], *Jingkun Jiang*[1,2], *Yu Song*[3], *Kaspar R. Daellenbach*[4,5], *Lu Qi*[4], *Andre S.H. Prevot*[4], *Jiming Hao*[1,2]

[1] *State Key Joint Laboratory of Environment Simulation and Pollution Control, School of Environment, Tsinghua University, Beijing 100084, China*

[2] *State Environmental Protection Key Laboratory of Sources and Control of Air Pollution Complex, Beijing 100084, China*

[3] *State Key Joint Laboratory of Environment Simulation and Pollution Control, Department of Environmental Science, Peking University, Beijing 100871, China*

[4] *Laboratory of Atmospheric Chemistry, Paul Scherrer Institute, 5232 Villigen, Switzerland*

[5] *Institute for Atmospheric and Earth System Research, University of Helsinki, Finland*

ARTICLE INFO

Article history:
Received 23 October 2019
Revised 3 April 2020
Accepted 3 April 2020
Available online 16 April 2020

Keywords:
Suburban Beijing
$PM_{2.5}$
WSOA (Water-soluble organic aerosol)
Offline-AMS (aerosol mass spectrometer) analysis
Source apportionment

ABSTRACT

$PM_{2.5}$ filter sampling and components measurement were conducted in autumn and winter from 2014 to 2015 at a suburban site (referred herein as "LLH site") located in the southwest of Beijing. The offline aerosol mass spectrometry (offline-AMS) analysis and positive matrix factorization (PMF) were applied for measurement and source apportionment of water-soluble organic aerosol (WSOA). Organic aerosol (OA) always dominated $PM_{2.5}$ during the sampling period, especially in winter. WSOA pollution was serious during the polluted period both in autumn (31.1 μg/m^3) and winter (31.9 μg/m^3), while WSOA accounted for 54.4% of OA during the polluted period in autumn, much more than that (21.3%) in winter. The oxidation degree of WSOA at LLH site was at a high level (oxygen-to-carbon ratio, O/C=0.91) and secondary organic aerosol (SOA) contributed more mass ratio of WSOA than primary organic aerosol (POA) during the whole observation period. In winter, coal combustion OA (CCOA) was a stable source of OA and on average accounted for 25.1% of WSOA. In autumn, biomass burning OA (BBOA) from household combustion contributed 38.3% of WSOA during polluted period. In addition to oxygenated OA (OOA), aqueous-oxygenated OA (aq-OOA) was identified as an important factor of SOA. During heavy pollution period, the mass proportion of aq-OOA to WSOA increased significantly, implying the significant SOA formation through

* Corresponding author.
E-mail: shxwang@tsinghua.edu.cn (S. Wang).
** These authors contributed equally to this work.

https://doi.org/10.1016/j.jes.2020.04.004

aqueous-phase process. The result of this study highlights the concentration on controlling the residential coal and biomass burning, as well as the research needs on aqueous chemistry in OA formation.

Introduction

In recent years, the heavy air pollution in northern China and its effect on human health have drawn more and more attentions. Beijing, the political and cultural center of China, has suffered from heavy pollution of fine particulate matter with aerodynamic diameter less than 2.5 μm ($PM_{2.5}$) along with the rapid economic growth and massive population (Guo et al., 2014; Zhang et al., 2014). Organic matter (OM, or organic aerosol, OA) contributes 20%-60% of the $PM_{2.5}$ mass and is considered as one of the main components of $PM_{2.5}$ (Duan et al., 2005; Hu et al., 2016; Huang et al., 2006; Sun et al., 2004; Takegawa et al., 2009; Zheng et al., 2005). Lots of field observations or laboratory researches have been carried out to investigate the characteristics and sources of OA in China, especially in Beijing (Elser et al., 2016; Huang et al., 2010; Sun et al., 2010; Sun et al., 2011, 2012, 2013, 2016; Xu et al., 2014; Xu et al., 2015b; Zhang et al., 2014; Zheng et al., 2015).

High-resolution time-of-flight aerosol mass spectrometer (HR-ToF-AMS, Aerodyne Research, Inc., USA), which couples thermal vaporization and mass spectrography, can provide quantitative mass spectra of non-refractory aerosol components (Canagaratna et al., 2007) and has been used to explore the chemical characteristics of fine particle OA. The factor-based receptor models, e.g., positive matrix factorization analysis (PMF), have been proven effective in apportioning OA into different factors representative of different pollution sources (Crippa et al., 2014; Jimenez et al., 2009; Lanz et al., 2007; Ng et al., 2010; Zhang et al., 2011). These factors include primary OA (POA, such as traffic related hydrocarbon-like OA (HOA), coal combustion OA (CCOA) and biomass burning OA (BBOA)) and secondary OA (SOA) which forms through the oxidation of volatile organic compounds (VOCs) or heterogeneous processes (Elser et al., 2016; Hu et al., 2016; Sun et al., 2012, 2013, 2015b; Zhang et al., 2014). Meanwhile, previous studies indicated the importance of SOA formation in the occurrence of haze events in megacities of China (Huang et al., 2014; Liu et al., 2013; Sun et al., 2014, 2016; Yang et al., 2015; Zhao et al., 2013). Water-soluble organic aerosol (WSOA) is often considered as a major component of OA, which significantly relates with SOA and consist of many oxidized species. Xiang et al. (2017) measured the water-soluble organic carbon (WSOC) in $PM_{2.5}$ filter samples at an urban site in Beijing from 2011 to 2012 and found that WSOC accounted for 26.6% of organinc carbon (OC). Xu et al. (2015a) even found high WSOC/OC ratio (0.79) in Tibet. Zhang et al. (2018b) conducted quantitative source apportionment of WSOC in four megacities of China including Beijing and declared that fossil fuel combustion contributed 32%-47% of WSOC on average and secondary organic carbon (SOC) dominated WSOC. Many studies have confirmed that both primary particles (mainly from biomass burning emissions) and SOA contributed to WSOA (Bozzetti et al., 2017a, 2017b; Kondo et al., 2007; Sannigrahi et al., 2006; Weber et al., 2007). However, in China, most previous studies focused on the concentration and chemical characteristics of WSOC (Tang et al., 2016; Xiang et al., 2017; Zhang et al., 2018b), which can not represent WSOA completely. Therefore, studies on the source apportionment, oxidation degree and formation mechanism of WSOA are still needed.

There are strong spatial variations of air quality in Beijing. The annual average $PM_{2.5}$ concentration in south Beijing was 30% higher than the average of the whole city in 2015 (Beijing Municipal Environmental Protection Bureau, 2016), but most previous studies referred before only focused on urban Beijing. Therefore, it is important to further investigate the chemical characteristics and source of WSOA in the southern suburb of Beijing. On the other hand, many studies in Beijing (Liang et al., 2015; Liu et al., 2015; Sun et al., 2013, 2014; Zhang et al., 2013) mainly paid attention to the air pollution in winter, but recent researches indicated that air pollution during autumn in Beijing can't be ignored (Xu et al., 2019; Zhang et al., 2018a).

In this study, field observations were carried out at a southwestern suburban site of Beijing to investigate the component characteristics and formation of WSOA in $PM_{2.5}$ both in autumn and winter. $PM_{2.5}$ samples were collected daily and the extracts of WSOA from these samples were measured by AMS. Source apportionment of WSOA was conducted using PMF method. The formation pathways and oxidation degree of WSOA were also analyzed. The result of this study may help identify the necessary actions to control WSOA pollution in Beijing and surrounding areas.

1. Field observation and analysis methods

1.1. *Site description, aerosol sampling and data collection*

The rural sampling site, Liulihe site (referred herein as "LLH site", 116°2′E and 39°36′N) is located at Fangshan District in the southwest of Beijing. LLH site is also located in the important southwest transport pathway of air pollution in Beijing-Tianjin-Hebei region (BTH). Detail information about the site was described in our previous studies (Hua et al., 2016, 2018). Ambient $PM_{2.5}$ were sampled by $PM_{2.5}/PM_{10}$ monitors (TEOM1405/1400a, Thermo Scientific, USA) with a flow rate of 10 L/min. The sampling was conducted from 10:00 am to 9:30 am of the next day with a duration time of 23 hr 30 min. The sampling periods included autumn (October 25th to November 18th, 2014) and winter (January 4th to February 3th, 2015).

Totally 31 valid $PM_{2.5}$ pre-baked (650°C for 8 hr to remove possibly adsorbed organic material) quartz fiber filters (47 mm, Whatman, Maidstone, UK) for chemical analysis and 31 valid $PM_{2.5}$ teflon filters (47 mm, Whatman, Maidstone, UK) for concentration calculation were collected (12 for autumn and 19 for winter, respectively). Some samples during the observation period were lacking because of instrument failure or samples being contaminated, so that they were not included in our study. Before analysis, all the loaded filters were wrapped in individual pre-baked (650°C for 8 hr) aluminum foil, sealed in polyethylene bags and stored in a refrigerator at −18°C in order to prevent the evaporation loss of volatile components. Field filter blanks were also conducted and stored following the same procedure for both seasons.

The meteorological parameters such as temperature (*T*), relative humidity (RH), wind speed (WS), wind direction (WD) and barometric pressure (*P*) were monitored by the near-

est meteorological monitoring site (to LLH site), i.e., National weather station of Zhuozhou. The data could be obtained from the Air Inquiry Website (http://q-weather.info/). Additionally, the concentrations of gaseous pollutants (NO_2, SO_2, O_3, CO) were measured by the Beijing air quality monitoring station at LLH. The data were downloaded from the website of Beijing environmental protection monitoring center (http://beijingair.sinaapp.com/). All of these hourly data were averaged into daily average.

The $PM_{2.5}$ mass was determined gravimetrically based on the teflon filters collected and using a digital balance (precision 0.01 mg, METTLER TOLEDO, Switzerland) in a laboratory with constant temperature and humidity before and after the sampling at least twice for accuracy. The daily equivalent sampling volumes at standard temperature and pressure (STP, 101,325 Pa and 273 K) were calculated from the volumetric data recorded by the $PM_{2.5}/PM_{10}$ monitors and the meteorological parameters mentioned above, then the daily average $PM_{2.5}$ concentrations were figured out.

1.2. *Offline-AMS analysis*

The offline-AMS analysis for WSOA of the quartz filters collected at LLH site was conducted in the Laboratory of Atmospheric Chemistry, Paul Scherrer Institute, 5232 Villigen, Switzerland where many studies based on AMS were carried out. A thorough and elaborative description of the offline-AMS analysis can be found in Daellenbach et al. (2016, 2017). Thus, here we only summarize it briefly.

For each quartz filter sample, four round punches with the diameter of 10 mm were submerged in a clean vial with 10 mL ultrapure water (18.2 MΩ•cm, total organic carbon < 5 ppb), sealed and subjected to ultrasound at 100 Hz and 0°C for 60 min to extract WSOA. The water extract was then filtered (0.45 μm nylon membrane syringe filters), sealed, stored in a thermotank with ice bags and transported to Paul Scherrer Institute. There the extract was aerosolized using a custom-built nebulizer with filtered synthetic air, dried by a silica gel diffusion dryer, and subsequently analyzed by a HR-ToF-AMS. The operating principles, calibration procedures, and analysis protocols of HR-ToF-AMS can be found in detail in DeCarlo et al. (2006). Particles are flash vaporized at 600°C and 10^{-7} Torr (1.3×10^{-5} Pa) in the instrument, and the generated gas is then ionized by electron impact (70 eV) to yield quantitative mass spectra of the non-refractory $PM_{1.0}$ (vacuum aerodynamic diameter (D_{va}) 60-600 nm) components. On average, 15 valid WSOA mass spectra per filter sample were collected and evaluated below (AMS V-mode, mass-to-charge ratio (usually referred as *m/z*) 12-300, 30-60 sec collection time per mass spectrum). Field blanks were also measured in a similar way as the collected sample filters. A system/measurement blank was conducted before every sample or field blank measurement by nebulizing ultrapure water for 12 min to monitor and reduce the possible memory effects.

Data of offline-AMS were processed and analyzed using high-resolution analysis fitting procedures, Squirrel v1.60 (SeQUential Igor data RetRiEvaL) and Pika v1.20 (Peak Integration by Key Analysis, D. Sueper), in the IGOR Pro software package (Wavemetrics, Inc., Portland, OR, USA). HR analysis of the AMS mass spectra in our work was performed in the mass range 12-115 D_{va} and in total 317 organic fragments were fitted. As described in Bozzetti et al. (2017a) and Daellenbach et al. (2017), the signal of CO_2^+ was corrected based on the measurements of standard NH_4NO_3 solution conducted routinely during the entire offline-AMS analysis period. Then, the organic CO^+ signal was set equal to organic CO_2^+, and organic H_2O^+, HO^+, and O^+ were scaled to CO_2^+ using the ratios proposed by Aiken et al. (2008): $H_2O^+ = 0.225 \times CO_2^+$, $HO^+ = 0.05625 \times CO_2^+$, and $O^+ = 0.009 \times CO_2^+$. Although some researches using argon as carrier gas found that organic CO_2^+ signal was about twice more than organic CO^+ signal (Bozzetti et al., 2017b; Ye et al., 2017), it would not influence the results too much if we set $CO^+ = 0.5 \times CO_2^+$, as shown in Appendix A Table S1. The measurement blank was subtracted from the sample and field blank mass spectra, that is, the valid signal (intensity) of every organic fragment is the difference between that of corresponding sample or field blank sample and that of measurement blank. The bulk WSOA properties such as elemental ratios including oxygen-to-carbon (*O/C*), hydrogen-to-carbon (*H/C*), nitrogen-to-carbon (*N/C*) ratios, and the organic mass-to-organic carbon (OM/OC_{AMS}) ratio can be obtained according to the method of Canagaratna et al. (2015).

1.3. *Other chemical analysis*

One 7 mm diameter punch from each quartz filter was treated using the same method as described above to extract water-soluble inorganic ions (WSIIs, including Cl^-, NO_3^-, SO_4^{2-}, NH_4^+, Na^+, K^+, Ca^{2+} and Mg^{2+}). The solution was then filtered with 0.45 μm Acrodisc syringe filters and analyzed by ion chromatography (Dionex ICS 600 and Dionex ICS 2100, Thermo Scientific, USA). One round punch (1 cm^2) was analyzed for elemental and organic carbon (EC and OC) using a thermal/optical carbon analyzer (Desert Research Institute (DRI) model 2001, Atmoslytic Inc, USA). The temperature steps of the Interagency Monitoring of Protected Visual Environments (IMPROVE) thermal evolution protocol was adopted, of which details can be referred to Xu et al. (2015a). WSOC mass was measured based on a standard method using the remaining part of the filter extracted in 40 mL ultrapure water in the same way as WSIIs, subsequently filtered and analyzed with a total organic carbon (TOC) analyzer (Multi N/C 3100, Analytic Jena AG, Germany) using high temperature (680°C) Pt-catalyzed oxidation coupled to non-dispersive infrared gas detection of CO_2. Then the ambient concentrations of these components could be converted. Daily aerosol liquid water (ALW) mass concentration was calculated using the available data of WSIIs and RH with the improved thermodynamic equilibrium aerosol model (ISORROPIA) (Fountoukis et al., 2007; Nenes et al., 1998).

It should be noted that all the filter blanks were treated using the same method, and data for the samples reported and analyzed below were blank corrected.

1.4. *Source apportionment of WSOA*

Source apportionment of the WSOA was performed using positive matrix factorization (PMF; Paatero and Tapper, 1994; Ulbrich et al., 2009) referring to many previous studies (Bozzetti et al., 2016, 2017b; Daellenbach et al., 2016, 2017; Ge et al., 2017). The PMF Evaluation Toolkit (PET v3.04) was employed and the PMF analysis protocol in Zhang et al. (2011) was followed. The significant variances among the samples allowed us to obtain physically meaningful PMF results.

However, the WSOA concentrations directly measured by AMS were dependent upon the concentrations of the liquid extracts and the flow rate of carrier gas, thus cannot represent original ambient mass loadings and needed to be converted. The real ambient WSOA concentrations with the unit of μg/m^3 were calculated by multiplying the ambient WSOC concentrations ($WSOC_{TOC}$, converted using the mass data from TOC analyzer and standard sampling volumes) with the OM/OC ratios obtained from the WSOA mass spectra (OM/OC_{AMS}), as shown in Eq. (1). The concentrations of water-insoluble organic aerosol (WIOA) can be calculated using Eq. (2), in which OC concentrations were determined by the thermal/optical carbon analyzer mentioned above, and 1.3 is the estimated

factor to convert water-insoluble organic carbon (WIOC) to organic mass according to Sun et al. (2011). Then, total OA concentrations can be obtained based on Eq. (3). The concentration of each fragment ($WSOA_i$, in μg/m^3) in WSOA was converted by multiplying the fraction of this signal intensity ($WSOA'_i$) in all the signal intensities with the estimated WSOA concentration, as shown in Eq. (4):

$$WSOA = WSOC_{TOC} \times OM/OC_{AMS} \quad (1)$$

$$WIOA = (OC - WSOC_{TOC}) \times 1.3 \quad (2)$$

$$OA = WSOA + WIOA \quad (3)$$

$$WSOA_i = WSOA \times \frac{WSOA'_i}{\sum WSOA'_i} \quad (4)$$

As mentioned before, the input PMF matrices for autumn and winter included 317 organic fragments fitted in the mass range 12–115 in this work. Each filter sample was represented by on average 15 valid high-resolution mass spectra, corrected for the corresponding average blank measured. Therefore, the matrix total dimension of LLH site was 179 × 317 = 56,743 in autumn and 354 × 317 = 112,218 in winter, respectively. The corresponding error matrices, in which the elements included the uncertainties related to the AMS measurements (Allan et al., 2003; Ulbrich et al., 2009) and the preceding blank variability as described in detail in Daellenbach et al. (2016), had the same dimensions. Prior to PMF execution, the input data and error matrices for WSOA, from which the field blank was subtracted, were both adjusted based on Eq. (4). All the elements in the input matrices and outcome were with the unit of μg/m^3. All isotopic ions were removed since their signals were not measured directly but scaled to their parent ions. Ions with a low signal-to-noise ratio (SNR < 0.2) were removed, and "weak" variables (0.2 < SNR < 2) were down-weighted by a factor of 3. The contributions of CO^+, H_2O^+, HO^+ and O^+ were also down-weighted according to Ulbrich et al. (2009) as their signals were scaled to CO_2^+. The PMF solutions were explored by varying the factors from 2 to 6 and the rotational forcing parameter (f_{peak}) from −1 to 1 with an increment of 0.1. After a thorough and careful evaluations of the solutions, comparing the mass spectra of the factors from different solutions with previously reported mass spectra, and analyzing the correlation between the time series of the factors with external tracers, different four-factor solutions with $f_{peak} = 0$ were chosen as the best solution for LLH site in autumn and winter, respectively. The details of the solutions are discussed in the following section.

2. Results and discussion

2.1. *Mass concentrations and chemical compositions of $PM_{2.5}$*

Appendix A Table S2 summarizes the average mass concentrations and chemical components of $PM_{2.5}$, concentrations of gaseous pollutants, temperature (*T*), and relative humidity (RH) at LLH site in different sampling periods. The whole sampling period was divided into clean or lightly polluted period and polluted period according to the different pollution characteristics. During clean or lightly polluted period, daily $PM_{2.5}$ concentration was lower than 115 μg/m^3 and average CO concentration was low as well (e.g., 1.0 mg/m^3 in autumn), indicating that meteorological condition was favorable for atmospheric diffusion. During polluted period, $PM_{2.5}$ pollution was severe (≥ 115 μg/m^3).

Overall, the $PM_{2.5}$ pollution was heavy at LLH site. The average $PM_{2.5}$ mass concentration was 100.4 μg/m^3 in autumn and 169.1 μg/m^3 in winter, respectively, much higher than the annual average level (83.3 μg/m^3) in urban Beijing in 2014. The $PM_{2.5}$ concentration during polluted period (163.3 μg/m^3 in autumn and 214.5 μg/m^3 in winter) was more than twice of that during clean or lightly polluted period, and far exceeded the China's national ambient air quality standards (e.g., 75 μg/m^3 for 24 hr average). The mass ratios of main chemical components in $PM_{2.5}$ are displayed in Fig. 1. It can be seen that OM and WSIIs both contributed to $PM_{2.5}$, and OM always dominated $PM_{2.5}$. WSIIs were dominated by nitrate, especially during polluted period in autumn (nitrate/WSIIs > 40%), which is consistent with the reported nitrate-driven haze pollution in north China, especially in urban Beijing (Xu et al., 2019; Zhang et al., 2018b). OM accounted for 50%–75% of $PM_{2.5}$ mass during the whole period, much higher than the reported values in urban Beijing (OM/$PM_{2.5}$: 20%–60%). During polluted period in winter, OM concentrations even reached 149.6 μg/m^3. That was possibly due to the large amount of primary OA emitted from coal combustion for heating in winter (Cai et al., 2018; Elser et al., 2016; Sun et al., 2014, 2016).

The average mass concentration of WSOA was 18.0 μg/m^3 in autumn and 24.7 μg/m^3 in winter, respectively, similar to the reported values (18.1 μg/m^3 in autumn and 25.1 μg/m^3 in winter) by offline-AMS analysis in Changzhou, China (Xiang et al., 2017), but much higher than that (4.9 μg/m^3 in winter) in southeastern rural USA (Sun et al., 2011) and that (14.6 μg/m^3) on average for autumn, winter and spring in urban Yangzhou, China (Ge et al., 2017). It is worth noting that WSOA (31.1 μg/m^3) accounted for 54.4% of OM during polluted period in autumn. However, in winter, the proportion of WSOA to OM in haze events decreased to 21.3%. That might be due to the large quantity of primary OA emission from coal combustion, which was usually considered less water soluble but contributed to major fraction of total OM in winter. Previous studies have verified coal combustion contributed a large proportion to primary OA in winter of Beijing (Sun et al., 2014, 2016; Zhang et al., 2014) but many primary OA could not be classified into WSOA (Bozzetti et al., 2017a, 2017b). Meanwhile, emissions from biomass combustion, an important source of WSOA, might decrease in winter compared with those in autumn. In addition, secondary formation processes in different seasons could also influence WSOA pollution. For example, the higher average RH value during polluted period (65% in autumn; 54% in winter) than that during clean or lightly polluted period implies the correlation between haze events and water vapor, suggesting the importance of aqueous-phase process of aerosol formation and evolution.

The time series of meteorological condition, concentrations of gaseous pollutants and $PM_{2.5}$ chemical components in two seasons at LLH site are shown in Fig. 2. The peak value of $PM_{2.5}$ concentrations was observed on November 18th in autumn, with a peak value of WSOA (47.9 μg/m^3). The mass ratio of WSOA to total OM (68.6%) on November 18th was also the highest value during the sampling period. However, RH was not very high (57%) and ALW concentration was only 6.0 μg/m^3 that day. The concentration of potassium ion (K^+), which could be considered as a tracer of biomass burning emission (Ng et al., 2010), was 2.1 μg/m^3, the peak value among all autumn samples. Meanwhile, higher daily O_x (= NO_2 + O_3) concentration (O_x: 114.6; NO_2: 97.7; O_3: 16.8 μg/m^3) than other days was also observed. Such phenomena verify that high WSOA concentration in this typical autumn haze event is subject to the contribution of biomass burning and aged SOA formation

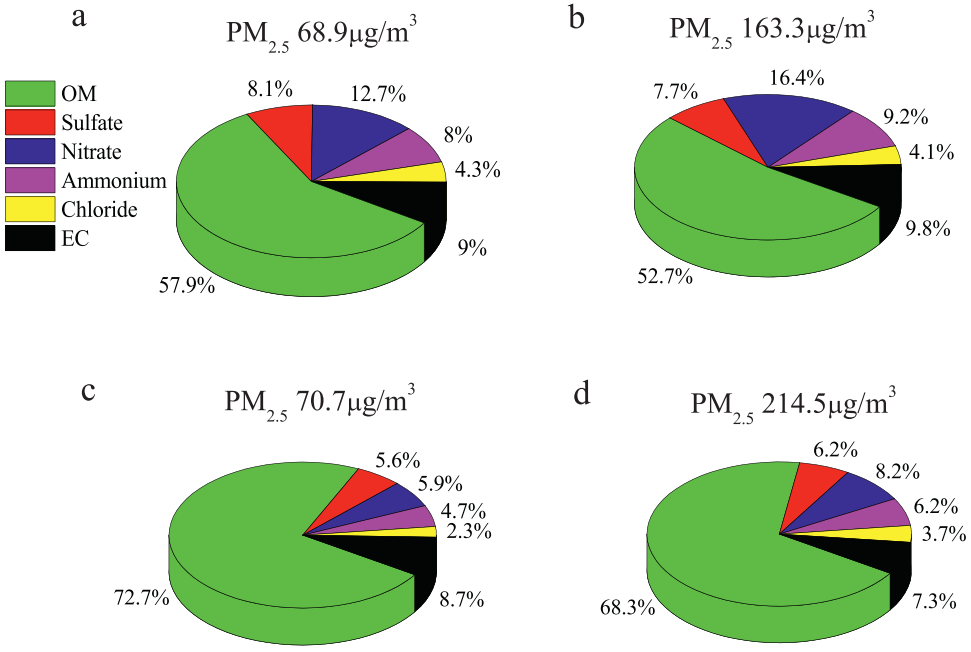

Fig. 1 – Mass ratios of the main chemical components of $PM_{2.5}$ at Liulihe (LLH) site during (a) clean or lightly polluted period in autumn, (b) polluted period in autumn, (c) clean or lightly polluted period in winter, and (d) polluted period in winter. OM: organic matter; EC: elemental carbon.

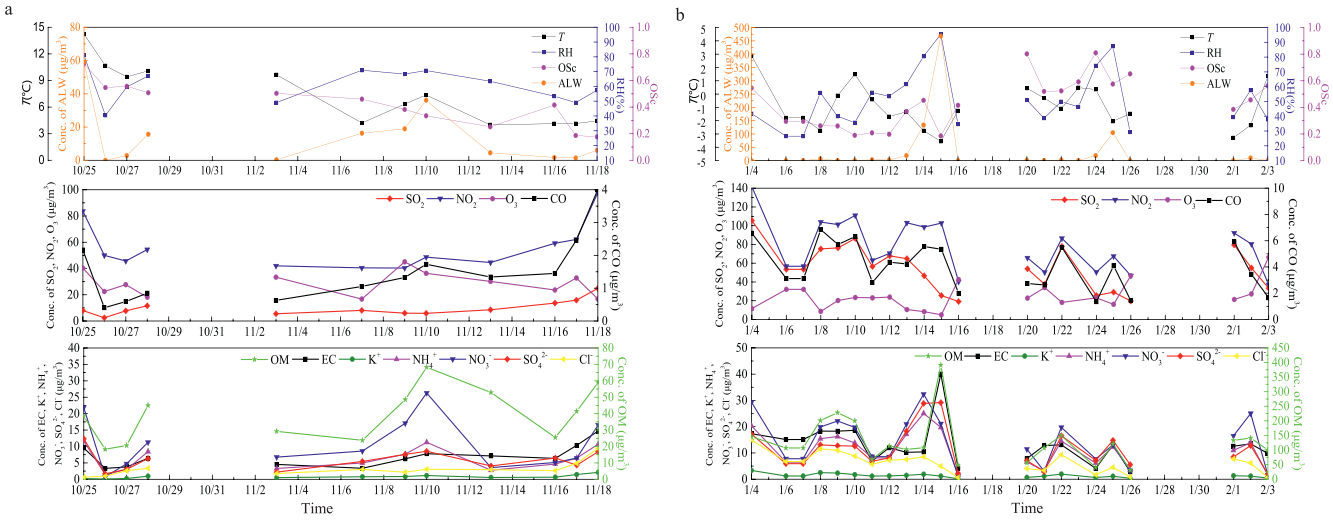

Fig. 2 – Time series of meteorological condition, gaseous pollutants and $PM_{2.5}$ chemical components at LLH site in (a) autumn and (b) winter. The lacking data were due to instrument failure or samples being contaminated. Conc.: concentration; T: temperature; RH: relative humidity; OSc: oxidation state of carbon; ALW: aerosol liquid water.

promoted by oxidizing gas. In winter, the most severe $PM_{2.5}$ pollution occurred on January 15th, also with the peak value of WSOA (90.8 μg/m^3). Different from that in autumn, it was a typical fog-haze event with high RH up to 95% and ALW concentration up to 468.1 μg/m^3, indicating that aqueous-phase process possibly played an important role in the formation of aerosols. At the same time, the EC concentration (40.0 μg/m^3) and SO_4^{2-} concentration (29.2 μg/m^3) were both very high, which implies the significant impact from coal combustion and transformation of SO_2 to SO_4^{2-} in liquid phase. In a word, for the typical fog-haze event in winter, primary sources (e.g., coal combustion) and aqueous reaction might be the key factors affecting WSOA formation.

2.2. *Sources of WSOA*

The difference between the chemical compositions of WSOA in autumn and those in winter implies different emission sources and formation pathways. As a premise, hydrocarbon-like OA (HOA) was proved poorly soluble in water (Daellenbach et al., 2016; Xu et al., 2017), therefore it is not considered in this study. In autumn, the four OA factors identified include two secondary OA factors, aqueous-oxygenated OA (aq-OOA) and oxygenated OA (OOA), and two primary OA factors, biomass burning OA (BBOA) and primary OA (POA, as an appellation of a factor, not representing any single source). In winter, the four OA factors are aq-OOA,

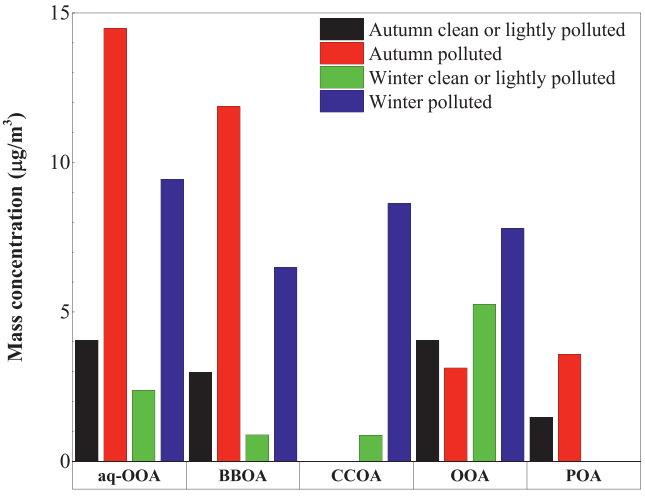

Fig. 3 – Average mass concentrations of OA factors during different periods at LLH site. aq-OOA: aqueous-oxygenated organic aerosol; BBOA: biomass burning organic aerosol; CCOA: coal combustion organic aerosol; OOA: oxygenated organic aerosol; POA: primary organic aerosol.

OOA, BBOA and coal combustion OA (CCOA). Fig. 3 shows the estimated average mass concentrations of these OA factors by PMF analysis during different periods at LLH site (detail data are given in Appendix A Table S3). Generally, in autumn, BBOA (32.8% of WSOA) and aq-OOA (41.7% of WSOA) were two main components of WSOA while the average concentration of OOA and POA were relatively low (< 4.0 μg/m^3). In contrast, the four OA factors contributed a relatively even proportion to WSOA in winter.

The mass spectra and elemental ratios of different OA factors at LLH site are shown in Figs. 4 and 5. Each OA factor was classified by spectral pattern and the comparison between the result in this study and those in relative researches. Time series of the OA factors are displayed in Fig. 6 to show the evolution of OA factors during the whole observation period. Triangular space (f_{44} vs. f_{43}, i.e., the fraction of *m/z* 44 and *m/z* 43 in certain total OA factor), as described in Ng et al. (2010) for analysis of oxidized OA, are plotted in Fig. 7 to show the oxidation degree of each OA factor. The location of the primary OA factors in this space implies that they had been oxidized to some extent. Detailed characteristics of different OA factors are described below.

2.2.1. *Coal combustion OA (CCOA)*

The mass spectrum of CCOA depends on the type of coal and oxygen/carbon ratios when burning (Wang et al., 2013). Despite of this, it is characterized by the presence of unsaturated hydrocarbons and strong polycyclic aromatic hydrocarbons (PAHs) fragment signatures, and shows relatively more significant signal at *m/z* 115 (mainly $C_9H_7^+$) (Elser et al., 2016; Sun et al., 2016). CCOA factor has been resolved by PMF analysis in winter in Beijing and is usually correlated with chloride (Elser et al., 2016; Hua et al., 2018; Sun et al., 2013). Also, previous studies showed that primary OA had strong correlation with CO emissions in urban area (de Gouw and Jimenez, 2009; Turpin and Huntzicker, 1995). In this study, there is the most significant signal at *m/z* 115 in CCOA spectrum (fraction of signal = 0.41%) among all the four factors in winter. The concentration of CCOA was verified highly correlated with PAHs signals, with R^2 between CCOA and $C_6H_3^+$, $C_7H_4^+$, $C_8H_5^+$, $C_9H_5^+$ fragments being 0.90, 0.91, 0.68, 0.89, respectively (Appendix A Fig. S1), which is consistent with the study of Sun et al. (2016). It also has a moderate correlation with that of chloride (R^2 = 0.67, see Appendix A Fig. S2a). In addition, the good correlation between CCOA and EC (R^2 = 0.79, see Appendix A Fig. S3) supports the identification of CCOA factor. Compared with EC and chloride, the correlation between CCOA and CO is weaker (R^2 = 0.51, see Appendix A Fig. S2b), which possibly is attributed to the influence of CO from regional transport and vehicle emissions at LLH site. Thus, CCOA factor was well identified in winter according to the consistence of its mass spectral characteristics with those in references mentioned above, but with more signal of *m/z* 44 (mostly CO_2^+). That is explicable because Zhou et al. (2016) found that *m/z* 44 and 73 can have significant changes during the different stages of coal burning. Fig. 7 also shows the oxidation degree of CCOA factor in our study was higher than other primary factors, which means that CCOA identified in WSOA had possibly been oxidized and contained more carboxylic acids than those freshly emitted.

On average, the concentration of CCOA during the whole winter observation at LLH site was 6.2 μg/m^3 (25.1% of WSOA). During polluted period at LLH site in winter, CCOA accounted for 27.0% of WSOA mass concentration, much higher than that during clean or lightly period (10.0%). It even dominated the WSOA loading (52.8%) on January 15th, the heaviest polluted day as mentioned above. On that day, the sudden sharp drop in temperature might result in more coal combustion for heating. Likewise, Elser et al. (2016) also observed the high contribution of CCOA to total OM (46.8%) during extreme haze periods in urban Beijing in January, 2014.

Actually, coal combustion is one of the main energy sources in China and is widely used for residential heating in northern China in winter. Since the implementation of the Action Plan on Air Pollution Prevention and Control in September 2013, the emission of coal combustion has been well-controlled in urban Beijing (Cheng et al., 2019; Ding et al., 2019). However, pollutant emissions from residential combustion can not be ignored before 2015, especially in suburb of Beijing. Cai et al (2018) reported that the annual usage of household coal for heating in LLH area in 2015 was 560 ton/km^2 and LLH area was one of the towns with most usage of coal-burning in Beijing. The annual $PM_{2.5}$ emission from household heating were over 8.0 ton in each village around LLH site. Thus, LLH site is a typical suburban site which was affected by residential coal combustion, especially in cold winter. In general, CCOA was a relatively stable primary factor of WSOA and had a great contribution to WSOA concentration during local emission-haze events in southwest suburb of Beijing in winter.

Nevertheless, CCOA was not identified in autumn at LLH site. Instead, the POA factor, which shows the mixed mass spectral pattern of CCOA and other primary OA with dominant signals of hydrocarbons, was identified in this study (Fig. 4). The average POA concentration was only 2.2 μg/m^3 during the whole autumn sampling period and the mass ratio of POA factor to WSOA was relatively stable in autumn (Fig. 6a). The oxidation degree of POA was the lowest (Fig. 7). These indicate that the primary OA emissions other than biomass burning were not key sources of WSOA pollution at LLH in autumn.

2.2.2. *Biomass burning OA (BBOA)*

BBOA has been resolved in autumn and winter in urban Beijing (Elser et al., 2016; Hu et al., 2016; Sun et al., 2016). In this study, BBOA factors were identified both in autumn and winter, and the mass spectra were similar to those resolved in northern Europe using offline-AMS (Bozzetti et al., 2017b). The same with previous studies, the mass spectra of BBOA in our study were characterized by prominent signals of *m/z* 60 (mainly $C_2H_4O_2^+$) and 73 (mainly $C_3H_5O_2^+$), which were considered as OA fragments indicative of biomass burning

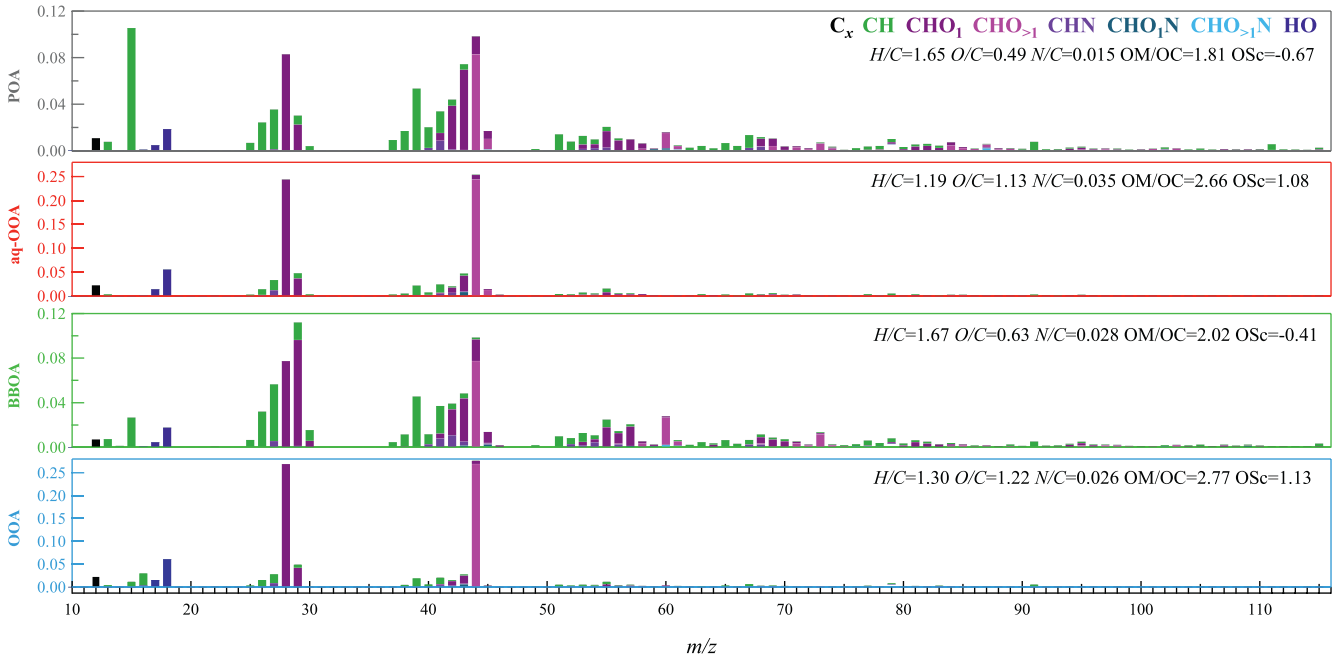

Fig. 4 – Spectra of different OA factors at LLH site in autumn. *H/C*: hydrogen-to-carbon ratio; *O/C*: oxygen-to-carbon ratio; *N/C*: nitrogen-to-carbon ratio; OM/OC: organic mass-to-organic carbon ratio; *m/z*: mass-to-charge ratio.

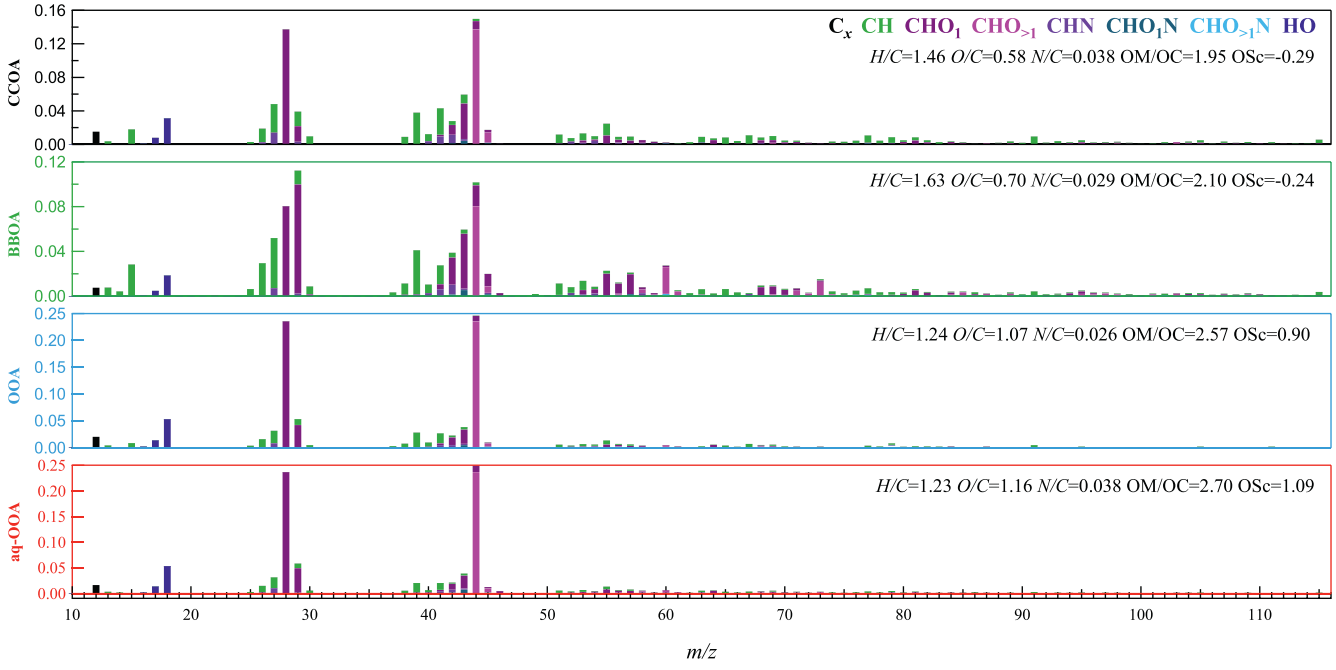

Fig. 5 – Spectra of different OA factors at LLH site in winter.

emission (Lanz et al., 2007; Mohr et al., 2009). The concentration of BBOA correlated well with that of $C_2H_4O_2^+$ ($R^2 = 0.99$ in autumn, $R^2 = 0.91$ in winter, see Appendix A Fig. S4). Also, the temporal variations of BBOA in autumn matched well with K^+ ($R^2 = 0.85$, see Appendix A Fig. S5a) which was usually regarded as biomass burning tracer. However, it showed a relatively weaker correlation with K^+ in winter ($R^2 = 0.65$, see Appendix A Fig. S5b), implying other emission sources of K^+ (e.g., fireworks and crustal materials) (Cheng et al., 2013). According to the Triangular space (f_{44} vs. f_{43}) plot, the oxidation degree of BBOA as a primary OA factor at LLH site was relatively low, which is desirable. The similar characteristic can be found in the triangular space (f_{CO2+} vs. f_{C2H3O+}) in the study of Bruns et al. (2015) focusing on wood combustion products. However, *O/C* of BBOA at LLH site was 0.63 in autumn and 0.70 in winter, much higher than that in other studies on ambient OA (Hu et al., 2016; Sun et al., 2016). Similar condition was found for *O/C* of CCOA. That's because the BBOA and CCOA factor discussed in this study were identified from WSOA rather than OA, and WSOA always is contributed by primary

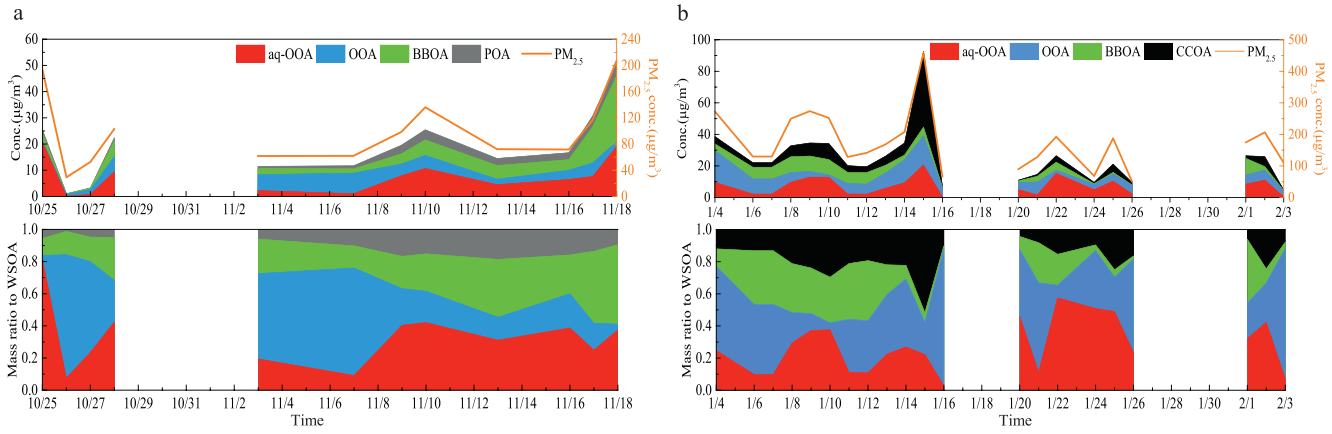

Fig. 6 – Time series of concentrations of OA factors at LLH site in (a) autumn and (b) winter. The lacking data were due to instrument failure or samples being contaminated. WSOA: water-soluble organic aerosol.

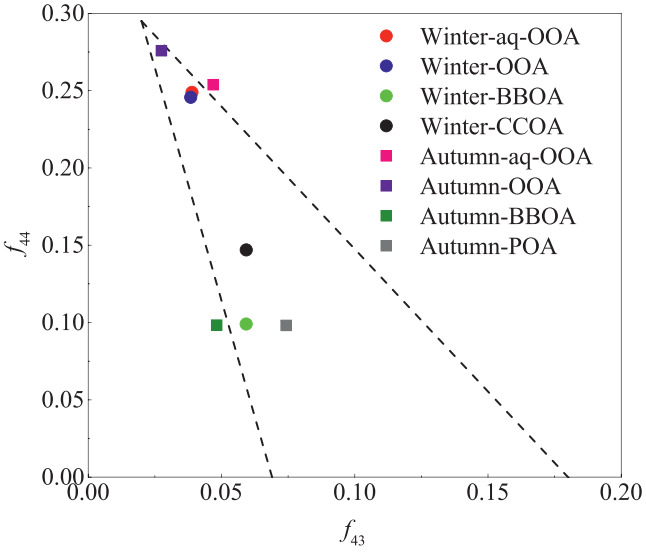

Fig. 7 – Triangular space (f_{44} vs. f_{43}, i.e., the fraction of *m/z* 44 and *m/z* 43 in certain total OA factor) for different OA factors at LLH site.

OA species with higher oxidation degree and aged SOA. Thus, the primary OA factors of WSOA should be considered as OA which had gone through oxidation process with higher *O/C* ratio. In addition, Bozzetti et al. (2017b) also found high OM/OC value of water soluble BBOA (1.88), slightly lower than the result of this study (2.02 in autumn and 2.10 in winter).

The average concentration of BBOA in WSOA at LLH site was 5.9 μg/m^3 in autumn and 4.7 μg/m^3 in winter, respectively, much higher than the value reported for central Europe (1.4 μg/m^3) (Daellenbach et al., 2017). It represented a relatively large fraction of WSOA, as shown in Fig. 6, especially in autumn (32.8%). During polluted period in autumn, BBOA dominated WSOA and its concentration was 11.9 μg/m^3 (38.3% of WSOA). Particularly on November 18th, BBOA concentration rose up to 25.1 μg/m^3 (52.4% of WSOA), indicating large effect from biomass burning. However, in winter, BBOA concentration decreased by almost half at LLH site (6.5 μg/m^3, 20.4% of WSOA during polluted period), which might explain the reduction of the fraction of WSOA in OM in winter since BBOA often shows good solubility in water (Daellenbach et al., 2016; Xu et al., 2017). Similarly, Hua et al. (2018) reported that BBOA contributed 20% to total OM in autumn but 13% in winter at LLH site based on aerosol chemical speciation monitor (ACSM)-PMF analysis. Elser et al. (2016) also found that BBOA accounted for less than 15% of total OM during extreme haze events in winter at an urban Beijing site. These results imply relatively less biomass burning activity in winter than that in autumn, which is different from the study in Europe (BBOA/OA = 43% in winter) (Bozzetti et al., 2017a).

Since there are many rural villages surrounding LLH site, wood combustion by households for cooking and heating purposes during cold weather could be a major source of BBOA (Wang et al., 2009). In North China Plain, rural people usually use coal and biomass together for cooking so it is difficult to distinguish them accurately, which could also explain the POA factor identified in autumn. The annual usage of biomass and coal for cooking was 16,400 ton of standard coal equivalent (tce) in LLH area, ranking the top towns with biomass and coal consumption for cooking in Beijing (Cai et al., 2018). That also explaines the large contribution from biomass burning to air pollution in rural Beijing.

Overall, the result of BBOA factor analysis suggests that BBOA always played an important role in WSOA formation in southwest suburban Beijing, especially in autumn, and it was mainly from residential cooking.

2.2.3. *Oxygenated OA (OOA) and aqueous-oxygenated OA (aq-OOA)*

OOA and aq-OOA are important SOA factors in this study and these two factors have been identified at LLH site both in autumn and winter. Aq-OOA is mainly part of oxygenated organic aerosol which forms through aqueous-phase process, and is influenced by many factors such as RH, particle-phase water, OH radicals, and inorganic salts (Huang et al., 2018; Lim et al., 2010; Wong et al., 2015). It has also been identified in winter in urban Beijing and was related with regional transport of pollutants (Hu et al., 2016; Sun et al., 2016; Wang et al., 2015; Xiang et al., 2017). As shown in Appendix A Fig. S6a, aq-OOA at LLH site has moderate to strong correlation with $C_2H_2O_2^+$ (*m/z* 58, $R^2 = 0.59$), $C_2O_2^+$ (*m/z* 56, $R^2 = 0.77$), $CH_2SO_2^+$ (*m/z* 78, $R^2 = 0.65$), $CH_3SO_2^+$ (*m/z* 79, $R^2 = 0.44$) and sulfate ($R^2 = 0.83$) in autumn, which has been verified in previous studies (Altieri et al., 2008; Carlton et al., 2007; Chhabra et al., 2010; Daellenbach et al., 2017; Sun et al., 2016; Tan et al., 2009). The correlations in winter (Appendix A Fig. S6b) are slightly weaker but still acceptable. $C_2H_2O_2^+$ and $C_2O_2^+$ are typical fragment ions of glyoxal and methylglyoxyal, which are impor-

Table 1 – Elemental analysis of WSOA or some factors in this and previous studies.

Research	Location	Chemical component	Season	H/C	O/C	N/C	OM/OC	OSc
This study	Rural	$PM_{2.5}$WSOA	Autumn	1.46	0.92	0.03	2.39	0.39
	Beijing		Winter	1.38	0.91	0.03	2.37	0.42
Xu et al., 2017	Rural Centreville	$PM_{1.0}$WSOA	Summer				2.05	
Sun et al., 2011	Southeastern	$PM_{2.5}$WSOA	Winter		0.59		1.98	
	USA		Summer		0.52		1.88	
Ye et al., 2017	Urban Changzhou	$PM_{2.5}$WSOA	Annual	1.69	0.54	0.11	1.99	
Zhang et al., 2012	Southeastern USA	$PM_{2.5}$WSOA	Annual				2	
Bozzetti et al., 2017a	Marseill	$PM_{2.5}$ BBOA	Annual		0.54		1.85	
		$PM_{2.5}$ OOA			0.51		1.82	
Daellenbach et al., 2017	Central	PM_{10} BBOA	Annual				1.74	
	Europe	PM_{10} SC-OA					1.82	
		PM_{10} SOOA					1.89	
		PM_{10} WOOA					2.12	
Ge et al., 2017	Urban	$PM_{2.5}$ BBOA	Annual	1.85	0.45	0.07	1.83	
	Yangzhou	$PM_{2.5}$ LOOOA		1.61	0.38	0.04	1.69	
		$PM_{2.5}$ MOOOA		1.49	0.78	0.06	2.24	
Sun et al., 2011	Southeastern	$PM_{2.5}$ LOOOA	Annual		0.5			
	USA	$PM_{2.5}$ MOOOA			0.6			
Ye et al., 2017	Urban	$PM_{2.5}$ MOOOA	Annual	1.28	1.2	0.05	2.77	
	Changzhou	$PM_{2.5}$ LOOOA		1.95	0.53	0.09	1.98	

SC-OA: sulfur-containing organic aerosol; SOOA: summer oxygenated organic aerosol; WOOA: winter oxygenated organic aerosol; LOOOA: less oxidized oxygenated OA; MOOOA: more oxidized oxygenated OA.

tant precursors of low volatile SOA in cloud process (Tan et al., 2009). $CH_2SO_2^+$ and $CH_3SO_2^+$ are typical fragment ions of methanesulfonic acid (MSA, CH_3SO_3H), a secondary product from the oxidation of dimethyl sulfide (DMS) through aqueous reactions (Ge et al., 2012; Zorn et al., 2008). In addition, daily aq-OOA concentration tracks well with ALW concentration ($R^2 = 0.73$ in autumn, except the data on November 18th when BBOA dominated the pollution; $R^2 = 0.74$ in winter, except the data on the days when RH < 50% referred to Sun et al. (2016), see Appendix A Fig. S7). These all verify that the resolved OA factor well represents aqueous-phase process of SOA formation. Similar with aq-OOA, OOA factor is characterized by high oxidation degree and prominent peak of *m/z* 44 (mostly CO_2^+). However, no significant correlation between OOA and external tracer species was found in this study, which is potentially because OOA factor represents many other formation pathways of SOA. Compared with Ng et al. (2010), the data points of OOA and aq-OOA in the triangle space shown in Fig. 7 imply the similarity between them and low-volatility oxidized OA (LV-OOA) and fulvic acid in previous researches.

In autumn, aq-OOA dominated SOA factors of WSOA (67.0% on average) and its concentration was 14.5 μg/m^3 (46.6% of WSOA) during polluted period at LLH site. OOA with a concentration of 3.1 μg/m^3 (10.0% of WSOA) was much lower compared with aq-OOA. Actually, the mass proportion of OOA to WSOA always decreased when the pollution became more severe at LLH site (OOA/WSOA ratio from clean or lightly polluted period to polluted period: 35.7% to 10.0% in autumn; 58.9% to 24.5% in winter). Instead, aq-OOA always drove the WSOA formation and increased sharply on the heavy polluted days (e.g., October 25th, 28th, November 10th and 18th, see Fig. 6a). However, slightly higher *O/C* of OOA factor (1.22) than that of aq-OOA factor (1.13) was observed (Fig. 4), which might be attributed to more significant promotion of photochemical reactions on the oxidation degree of OOA in autumn. On the other hand, aq-OOA showed a strong correlation with O_x ($R^2 = 0.81$, see Appendix A Fig. S8) in autumn, which indicates that ambient oxidizing gas may also promote aqueous reaction. Overall, in autumn, aqueous phase oxidation had much more significant influence on the yields of aged OA in haze events than other pathways such as photochemical reactions, which nevertheless could increase the oxidation degree of WSOA more.

As shown in Fig. 6b, the contribution of OOA also decreased in the haze events on January 8th-10th, 15th, 22th, and 25th in winter, but aq-OOA mass proportion increased. That could be considered as evidence for the aq-OOA driven SOA formation in some haze events at LLH site in winter. However, on average, OOA (28.3%) and aq-OOA (28.7%) have contributed together to WSOA during the whole winter observation period. In the study of Sun et al. (2016), OOA and aq-OOA on average contributed 32% and 12% to OA in winter in urban Beijing, respectively, which highlighted photochemical production. But it also reported that aq-OOA could contribute 37%-45% to total OA in some typical episodes with high RH, which is consistent with the event on January 22th (aq-OOA/WSOA: 57.7%) in this study. Actually, the lower temperature in winter of Beijing also facilitated the partitioning of semi-volatile oxidized species into particle phase, which may explain that OOA accounted for more WSOA mass in winter than in autumn. As for elemental analysis, in winter, *O/C* and *N/C* of aq-OOA (*O/C*: 1.16; *N/C*: 0.038) were both higher than those of OOA (*O/C*: 1.07; *N/C*: 0.026) at LLH site (Fig. 5). Higher *N/C* ratio (also found in autumn, 0.035 vs. 0.026, see Fig. 4) verifies that aqueous-phase process of glyoxal/methylglyoxal with amino acids and amines can form nitrogen-containing compounds (Ge et al., 2011), which is consistent with Sun et al. (2016). Higher *O/C* ratio of aq-OOA suggests that OA aging pathway by aqueous-phase process resulted in SOA with higher oxidation degree than other processes in winter, which is different from the condition in autumn.

In conclusion, aqueous-phase process had a significant influence on WSOA pollution (including concentration, composition and oxidation degree), and aq-OOA drove the SOA formation during haze events in southwest suburb of Beijing, especially in autumn.

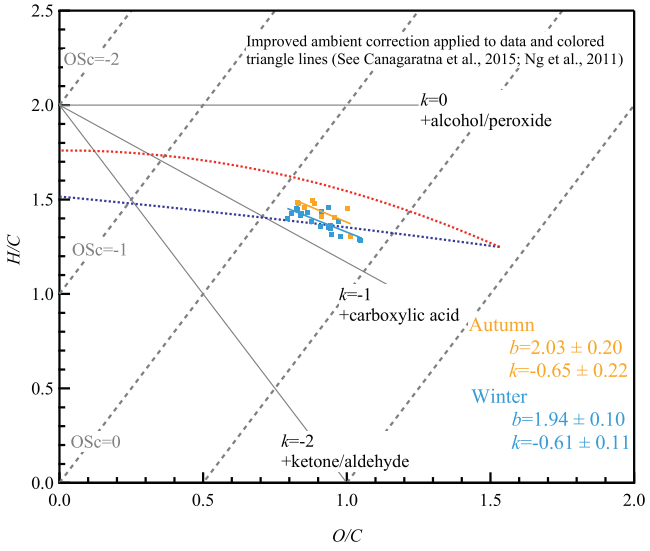

Fig. 8 – Van Krevelen diagram (V-K diagram) of WSOA at LLH site in autumn and winter. *k*: the slope of the fitting straight line; *b*: the intercept of the fitting straight line.

2.3. *Elemental analysis of WSOA*

The elemental analysis results of WSOA or some factors in this study and previous researches are shown in Table 1. The *O/C* ratio of WSOA were about 0.92 in autumn and 0.91 in winter at LLH site, much higher than that in other regions. Meanwhile, the average OM/OC ratio at LLH site was also at a higher level (on average about 2.38). The only exception is the result of the more-oxidized oxygenated OA (MO-OOA) factor in urban Changzhou, but that can't represent the average oxidation degree of total WSOA. Usually the OM/OC ratio of oxidized OA in remote areas (2.0–2.5) is higher than that in urban areas (Aiken et al., 2008; Hu et al., 2012; Hu et al., 2016). There is also research declaring that SOA formed through aqueous chemistry has *O/C* ratio of 1-2 (OM/OC ratio of 2.5-3.8), and oligomeric methylglyoxal have an average *O/C* ratio of 0.7-1.1 (OM/OC ratio of 2.0-2.6) (Lim et al., 2010). Oxidation state of carbon (OSc, defined as $2 \times O/C - H/C$) was regarded more useful to describe the oxidation degree of OA (Kroll et al., 2011; Mandariya et al., 2019; Wang et al., 2017). Thus, daily OSc at LLH site was calculated to show the oxidation degree of total WSOA (Fig. 2). Then, the Van Krevelen diagram (V-K diagram), in which the slope of the fitting straight line may describe the aging pathway of OA (Canagaratna et al., 2015; Ng et al., 2011), is given in Fig. 8. The steeper slopes (−0.65 in autumn; −0.61 in winter) of WSOA at LLH site than that of OA in urban Beijing (−0.43) (Zhang et al., 2014) imply the greater effect of the addition of carboxylic acid groups on the formation of WSOA in suburban Beijing.

In addition, as listed in Appendix A Table S3, SOA factors contributed to WSOA (62.2% in autumn, 57.1% in winter) much more than primary OA factors (including POA factor, CCOA factor and BBOA factor). On January 15th in winter, when coal combustion promoted the formation of water soluble CCOA, OOA and aq-OOA could still account for 43.1% of total WSOA. In contrast, primary OA accounted for 56%-75% mass concentration of total OA in winter in urban Beijing (Elser et al., 2016; Hu et al., 2016; Hua et al., 2018; Sun et al., 2016).

To summarize, the oxidation degree of WSOA in southwest suburb of Beijing both in autumn and winter was very high, mainly due to the high proportion of secondary formation through aqueous chemistry (e.g., oligomers) and aging reactions of OA (e.g., addition of carboxylic acid groups) in rural areas of Beijing.

3. Conclusions

The $PM_{2.5}$ chemical compositions and sources of WSOA in autumn and winter from 2014 to 2015 were comprehensively characterized based on particle samples measurement at LLH site in southwest suburb of Beijing. The result shows serious OA pollution, which accounted for 50%–75% of $PM_{2.5}$ mass during the whole observation period and was much more severe in winter than that in autumn. However, the proportion of WSOA with high oxidation degree in autumn (WSOA concentration: 18.0 μg/m^3, WSOA/OM: 43.9%) is higher than that in winter (WSOA concentration: 24.7 μg/m^3, WSOA/OM: 20.5%), suggestting attention to the formation pathways and control of WSOA in suburban Beijing.

Consequently, four OA factors were resolved by PMF analysis for autumn and winter, respectively. It is noted that the aq-OOA factor, representative of aqueous formation process of SOA, has been identified significantly. Overall, BBOA (32.8%) and aq-OOA (41.7%) were two main components of WSOA in autumn. All four OA factors contributed a relatively even proportion of WSOA in winter. Coal combustion was a relatively stable primary source of WSOA (25.1%) but sometimes could promote WSOA pollution during local emission-haze events in winter. Residential biomass burning activity played an important role in WSOA formation at LLH site, more significantly in autumn (11.9 μg/m^3) than in winter (6.5 μg/m^3) during polluted period. Compared with other pathways, aqueous-phase process might lead to more yield of SOA in southwest suburb of Beijing, especially in autumn. In winter, OA aging pathway by aqueous-phase process (e.g., the formation of oligomers and carboxylic acid groups) resulted in SOA with higher oxidation degree. While in autumn, the oxidation by more photochemical reactions might influence the oxidation degree of WSOA more significantly.

The findings of this study suggest that the clean energy replacement of household solid fuel, i.e., biomass burning in autumn and coal combustion in winter will be an effective way to reduce WSOA pollution in suburban Beijing. However, it is still unclear how oxidizing gas (O_x) influence aq-OOA and which organic precursors contribute greatly to it in BTH. Thus, further studies shall be conducted to investigate the aqueous reactions in heavy pollution events occurring in both urban and suburban areas in north China through observation and laboratory simulation.

Declaration of competing interest

We declare that we have no conflicts of interest to this work "Chemical Characteristics and Sources of Water-Soluble Organic Aerosol in southwest suburb of Beijing". We declare that we do not have any commercial or associative interest that represents a conflict of interest in connection with the work submitted.

Acknowledgments

This work was supported by the National Natural Science Foundation of China (No. 21625701) and the Beijing Municipal Science and Technology Project (No. Z181100005418018 and Z191100009119001). We acknowledge funding of the SNF

project "Source Apportionment of Organics in ambient air including Primary, Secondary Organic Aerosols and trace Gases (SAOPSOAG)" (No. 200021_169787).

Appendix A. Supplementary data

Supplementary material associated with this article can be found in the online version at doi:10.1016/j.jes.2020.04.004.

REFERENCES

Aiken, A.C., Decarlo, P.F., Kroll, J.H., Worsnop, D.R., Huffman, J.A., Docherty, K.S., et al., 2008. O/C and OM/OC ratios of primary, secondary, and ambient organic aerosols with high-resolution time-of-flight aerosol mass spectrometry. Environ. Sci. Technol. 42, 4478–4485.

Allan, J.D., Jimenez, J.L., Williams, P.I., Alfarra, M.R., Bower, K.N., Jayne, J.T., et al., 2003. Quantitative sampling using an Aerodyne aerosol mass spectrometer: 1. Techniques of data interpretation and error analysis. J. Geophys. Res. Atmos. 108 (D3), 4090.

Altieri, K.E., Seitzinger, S.P., Carlton, A.G., Turpin, B.J., Klein, G.C., Marshall, A.G., 2008. Oligomers formed through in-cloud methylglyoxal reactions: Chemical composition, properties, and mechanisms investigated by ultra-high resolution FT-ICR mass spectrometry. Atmos. Environ. 42, 1476–1490.

Beijing Municipal Environmental Protection Bureau, 2016. Beijing Environmental statement 2015. Available: http://sthjj.beijing.gov.cn/bjhrb/resource/cms/oldfile/bjepb/resource/cms/2016/04/201604180190124742.pdf Accessed September 25, 2019.

Bozzetti, C., Daellenbach, K.R., Hueglin, C., Fermo, P., Sciare, J., Kasper-Giebl, A., et al., 2016. Size-resolved identification, characterization and quantification of primary biological organic aerosol at a European rural site. Environ. Sci. Technol. 50, 13177–13178.

Bozzetti, C., El Haddad, I., Salameh, D., Daellenbach, K.R., Fermo, P., Gonzalez, R., et al., 2017a. Organic aerosol source apportionment by offline-AMS over a full year in Marseille. Atmos. Chem. Phys. 17, 8247–8268.

Bozzetti, C., Sosedova, Y., Xiao, M., Daellenbach, K.R., Ulevicius, V., Dudoitis, V., et al., 2017b. Argon offline-AMS source apportionment of organic aerosol over yearly cycles for an urban, rural, and marine site in northern Europe. Atmos. Chem. Phys. 17, 117–141.

Bruns, E.A., Krapf, M., Orasche, J., Huang, Y., Zimmermann, R., Drinovec, L., et al., 2015. Characterization of primary and secondary wood combustion products generated under different burner loads. Atmos. Chem. Phys. 15, 2825–2841.

Cai, S.Y., Li, Q., Wang, S.X., Chen, J.M., Ding, D.A., Zhao, B., et al., 2018. Pollutant emissions from residential combustion and reduction strategies estimated via a village-based emission inventory in Beijing. Environ. Pollut. 238, 230–237.

Canagaratna, M.R., Jayne, J.T., Jimenez, J.L., Allan, J.D., Alfarra, M.R., Zhang, Q., et al., 2007. Chemical and microphysical characterization of aerosols via aerosol mass spectrometry. Mass Spectrom. Rev. 26, 185–222.

Canagaratna, M.R., Jimenez, J.L., Kroll, J.H., Chen, Q., Kessler, S.H., Massoli, P., et al., 2015. Elemental ratio measurements of organic compounds using aerosol mass spectrometry: characterization, improved calibration, and implications. Atmos. Chem. Phys. 15, 253–272.

Carlton, A.G., Turpin, B.J., Altieri, K.E., Seitzinger, S., Reff, A., Lim, H.-J., et al., 2007. Atmospheric oxalic acid and SOA production from glyoxal: Results of aqueous photooxidation experiments. Atmos. Environ 41, 7588–7602.

Cheng, J., Su, J.P., Cui, T., Li, X., Dong, X., Sun, F., et al., 2019. Dominant role of emission reduction in $PM_{2.5}$ air quality improvement in Beijing during 2013-2017: a model-based decomposition analysis. Atmos. Chem. Phys. 19, 6125–6146.

Cheng, Y., Engling, G., He, K.B., Duan, F.K., Ma, Y.L., Du, Z.Y., et al., 2013. Biomass burning contribution to Beijing aerosol. Atmos. Chem. Phys. 13, 7765–7781.

Chhabra, P.S., Flagan, R.C., Seinfeld, J.H., 2010. Elemental analysis of chamber organic aerosol using an aerodyne high-resolution aerosol mass spectrometer. Atmos. Chem. Phys. 10, 4111–4131.

Crippa, M., Canonaco, F., Lanz, V.A., Aijala, M., Allan, J.D., Carbone, S., et al., 2014. Organic aerosol components derived from 25 AMS data sets across Europe using a consistent ME-2 based source apportionment approach. Atmos. Chem. Phys. 14, 6159–6176.

Daellenbach, K.R., Bozzetti, C., Krepelova, A.K., Canonaco, F., Wolf, R., Zotter, P., et al., 2016. Characterization and source apportionment of organic aerosol using offline aerosol mass spectrometry. Atmos. Meas. Tech. 9, 23–39.

Daellenbach, K.R., Stefeneli, G., Bozzetti, C., Vlachou, A., Fermo, P., Gonzalez, R., et al., 2017. Long-term chemical analysis and organic aerosol source apportionment at nine sites in central Europe: source identification and uncertainty assessment. Atmos. Chem. Phys. 17, 13265–13282.

de Gouw, J., Jimenez, J.L., 2009. Organic aerosols in the Earth's atmosphere. Environ. Sci. Technol 43, 7614–7618.

Decarlo, P.F., Kimmel, J.R., Trimborn, A., Northway, M.J., Jayne, J.T., Aiken, A.C., et al., 2006. Field-deployable, high-resolution, time-of-flight aerosol mass spectrometer. Anal. Chem. 78, 8281–8289.

Ding, D., Xing, J., Wang, S.X., Liu, K.Y., Hao, J.M., 2019. Estimated contributions of emissions controls, meteorological factors, population growth, and changes in baseline mortality to reductions in ambient $PM_{2.5}$ and $PM_{2.5}$-related mortality in China, 2013-2017. Environ. Health Persp. 127, 067009.

Duan, F.K., He, K.B., Ma, Y.L., Jia, Y.T., Yang, F.M., Lei, Y., et al., 2005. Characteristics of carbonaceous aerosols in Beijing, China. Chemosphere 60, 355–364.

Elser, M., Huang, R.J., Wolf, R., Slowik, J.G., Wang, Q.Y., Canonaco, F., et al., 2016. New insights into $PM_{2.5}$ chemical composition and sources in two major cities in China during extreme haze events using aerosol mass spectrometry. Atmos. Chem. Phys. 16, 3207–3225.

Fountoukis, C., Nenes, A., Meskhidze, N., Bahreini, R., Seinfeld, J.H., 2007. Aerosol-cloud drop concentration closure for clouds sampled during the international consortium for atmospheric research on transport and transformation 2004 campaign. J. Geophys. Res.-Atmos. 112, 1–12.

Ge, X.L., Wexler, A.S., Clegg, S.L., 2011. Atmospheric Amines –Part II. Thermodynamic properties and gas/particle partitioning. Atmos. Environ. 45, 561–577.

Ge, X.L., Ruehl, C.R., Sun, Y.L., Ruehl, C.R., Setyan, A., 2012. Effect of aqueous-phase processingon aerosolchemistry and sizedistributions in Fresno, California, during wintertime. Environ. Chem. 9, 221–235.

Ge, X.L., Li, L., Chen, Y.F., Chen, H., Wu, D., Wang, J.F., et al., 2017. Aerosol characteristics and sources in Yangzhou, China resolved by offline aerosol mass spectrometry and other techniques. Environ. Pollut. 225, 74–85.

Guo, S., Hu, M., Zamora, M.L., Peng, J.F., Shang, D.J., Zheng, J., et al., 2014. Elucidating severe urban haze formation in China. Proc. Natl. Acad. Sci. USA 111, 17373–17378.

Hu, W.W., Hu, M., Deng, Z.Q., Xiao, R., Kondo, Y., Takegawa, N., et al., 2012. The characteristics and origins of carbonaceous aerosol at a rural site of PRD in summer of 2006. Atmos. Chem. Phys. 12, 1811–1822.

Hu, W.W., Hu, M., Hu, W., Jimenez, J.L., Yuan, B., Chen, W.T., et al., 2016. Chemical composition, sources and aging process of submicron aerosols in Beijing: contrast between summer and winter. J. Geophys. Res. Atmos. 121, 1955–1977.

Hua, Y., Wang, S.X., Wang, J.D., J.k., Jiang, Zhang, T., Song, Y., 2016. Investigating the impact of regional transport on $PM_{2.5}$ formation using vertical observation during APEC 2014 Summit in Beijing. Atmos. Chem. Phys. 16 (24), 15451–15460.

Hua, Y., Wang, S.X., Jiang, J.K., Zhou, W., Xu, Q.C., Li, X.X., et al., 2018. Characteristics and sources of aerosol pollution at a polluted rural site southwest in Beijing, China. Sci. Total Environ. 626, 519–527.

Huang, D.D., Zhang, Q., Cheung, H.H.Y., Yu, L., Zhou, S., Anastasio, C., et al., 2018. Formation and evolution of aqSOA from aqueous-phase reactions of phenolic carbonyls: Comparison between ammonium sulfate and ammonium nitrate solutions. Environ. Sci. Technol. 52, 9215–9224.

Huang, R.J., Zhang, Y.L., Bozzetti, C., Ho, K.F., Cao, J.J., Han, Y.M., et al., 2014. High secondary aerosol contribution to particulate pollution during haze events in China. Nature 514, 218–222.

Huang, X.F., He, L.Y., Hu, M., Zhang, Y.H., 2006. Annual variation of particulate organic compounds in $PM_{2.5}$ in the urban atmosphere of Beijing. Atmos. Environ. 40, 2449–2458.

Huang, X.F., He, L.Y., Hu, M., Canagaratna, M.R., Sun, Y., Zhang, Q., et al., 2010. Highly time-resolved chemical characterization of atmospheric submicron particles during 2008 Beijing Olympic Games using an aerodyne high-resolution aerosol mass spectrometer. Atmos. Chem. Phys. 10, 8933–8945.

Jimenez, J.L., Canagaratna, M.R., Donahue, N.M., Prevot, A.S.H., Zhang, Q., Kroll, J.H., et al., 2009. Evolution of organic aerosols in the atmosphere. Science 326, 1525–1529.

Kondo, Y., Miyazaki, Y., Takegawa, N., Miyakawa, T., Weber, R.J., Jimenez, J.L., et al., 2007. Oxygenated and water-soluble organic aerosols in Tokyo. J. Geophys. Res.-Atmos. 112, D01203.

Kroll, J.H., Donahue, N.M., Jimenez, J.L., Kessler, S.H., Canagaratna, M.R., Wilson, K.R., et al., 2011. Carbon oxidation state as a metric for describing the chemistry of atmospheric organic aerosol. Nat. Chem. 3, 133–139.

Lanz, V.A., Alfarra, M.R., Baltensperger, U., Buchmann, B., Hueglin, C., Prevot, A.S.H., 2007. Source apportionment of submicron organic aerosols at an urban site by factor analytical modelling of aerosol mass spectra. Atmos. Chem. Phys. 7, 1503–1522.

Liang, X., Zou, T., Guo, B., Li, S., Zhang, H.Z., Zhang, S.Y., et al., 2015. Assessing Beijing's $PM_{2.5}$ pollution: severity, weather impact, APEC and winter heating. Proc. Roy. Soc. A-Math. Phy. 471, 20150257.

Lim, Y.B., Tan, Y., Perri, M.J., Seitzinger, S.P., Turpin, B.J., 2010. Aqueous chemistry and its role in secondary organic aerosol (SOA) formation. Atmos. Chem. Phys. 10, 10521–10539.

Liu, X.G., Li, J., Qu, Y., Han, T., Hou, L., Gu, J., et al., 2013. Formation and evolution mechanism of regional haze: a case study in the megacity Beijing, China. Atmos. Chem. Phys. 13, 4501–4514.

Liu, Z.R., Hu, B., Wang, L.L., Wu, F.K., Gao, W.K., Wang, Y.S., 2015. Seasonal and diurnal variation in particulate matter (PM_{10} and $PM_{2.5}$) at an urban site of Beijing: analyses from a 9-year study. Environ. Sci. Pollut. R. 22, 627–642.

Mandariya, A.K., Gupta, T., Tripathi, S.N., 2019. Effect of aqueous-phase process on the formation and evolution of organic aerosol (OA) under different stages of fog life cycles. Atmos. Environ. 206, 60–71.

Mohr, C., Huffman, J.A., Cubison, M.J., Aiken, A.C., Docherty, K.S., Kimmel, J.R., et al., 2009. Characterization of primary organic aerosol emissions from meat cooking, trash burning, and motor vehicles with high-resolution aerosol mass

spectrometry and comparison with ambient and chamber observations. Environ. Sci. Technol. 43, 2443–2449.
Nenes, A., Pandis, S.N., Pilinis, C., 1998. ISORROPIA: A new thermodynamic equilibrium model for multiphase multicomponent inorganic aerosols. Aquat. Geochem. 4, 123–152.
Ng, N.L., Canagaratna, M.R., Zhang, Q., Jimenez, J.L., Tian, J., Ulbrich, I.M., et al., 2010. Organic aerosol components observed in Northern Hemispheric datasets from aerosol mass spectrometry. Atmos. Chem. Phys. 10, 4625–4641.
Ng, N.L., Canagaratna, M.R., Jimenez, J.L., Chhabra, P.S., Seinfeld, J.H., Worsnop, D.R., 2011. Changes in organic aerosol composition with aging inferred from aerosol mass spectra. Atmos. Chem. Phys. 11, 6465–6474.
Paatero, P., Tapper, U., 1994. Positive Matrix Factorization - a nonnegative factor model with optimal utilization of error-estimates of data values. Environmetrics 5, 111–126.
Sannigrahi, P., Sullivan, A.P., Weber, R.J., Ingall, E.D., 2006. Characterization of water-soluble organic carbon in urban atmospheric aerosols using solid-state C-13NMR spectroscopy. Environ. Sci. Technol. 40, 666–672.
Sun, J.Y., Zhang, Q., Canagaratna, M.R., Zhang, Y.M., Ng, N.L., Sun, Y.L., et al., 2010. Highly time- and size-resolved characterization of submicron aerosol particles in Beijing using an Aerodyne aerosol mass spectrometer. Atmos. Environ. 44, 131–140.
Sun, Y.L., Zhuang, G.S., Ying, W., Han, L.H., Guo, J.H., Mo, D., et al., 2004. The air-borne particulate pollution in Beijing-Concentration, composition, distribution and sources. Atmos. Environ. 38, 5991–6004.
Sun, Y.L., Zhang, Q., Zheng, M., Ding, X., Edgerton, E.S., Wang, X.M., 2011. Characterization and source apportionment of water-soluble organic matter in atmospheric fine particles ($PM_{2.5}$) with high-resolution aerosol mass spectrometry and GC–MS. Environ. Sci. Technol. 45, 4854–4861.
Sun, Y.L., Wang, Z.F., Dong, H.B., Yang, T., Li, J., Pan, X.L., et al., 2012. Characterization of summer organic and inorganic aerosols in Beijing, China with an aerosol chemical speciation monitor. Atmos. Environ. 51, 250–259.
Sun, Y.L., Wang, Z.F., Fu, P.Q., Yang, T., Jiang, Q., Dong, H.B., et al., 2013. Aerosol composition, sources and processes during wintertime in Beijing, China. Atmos. Chem. Phys. 13, 4577–4592.
Sun, Y.L., Jiang, Q., Wang, Z.F., Fu, P.Q., Li, J., Yang, T., et al., 2014. Investigation of the sources and evolution processes of severe haze pollution in Beijing in January 2013. J. Geophys. Res. Atmos. 119, 4380–4398.
Sun, Y.L., Du, W., Fu, P.Q., Wang, Q.Q., Li, J., Ge, X.L., et al., 2016. . Primary and secondary aerosols in Beijing in winter: sources, variations and processes. Atmos. Chem. Phys. 16, 8309–8329.
Tan, Y., Perri, M.J., Seitzinger, S.P., Turpin, B.J., 2009. Effects of precursor concentration and acidic sulfate in aqueous glyoxal-OH radical oxidation and implications for secondary organic aerosol. Environ. Sci. Technol. 43, 8105–8112.
Tang, X., Zhang, X.S., Wang, Z.W., Ci, Z.J., 2016. Water-soluble organic carbon (WSOC) and its temperature-resolved carbon fractions in atmospheric aerosols in Beijing. Atmos. Res. 181, 200–210.
Takegawa, N., Miyakawa, T., Kuwata, M., Kondo, Y., Zhao, Y., Han, S., et al., 2009. Variability of submicron aerosol observed at a rural site in Beijing in the summer of 2006. J. Geophys. Res. Atmos. 114, D00G05.
Turpin, B.J., Huntzicker, J.J., 1995. Identification of secondary organic aerosol episodes and quantitation of primary and secondary organic aerosol concentrations during Scaqs. Atmos. Environ. 29, 3527–3544.
Ulbrich, I.M., Canagaratna, M.R., Zhang, Q., Worsnop, D.R., Jimenez, J.L., 2009. Interpretation of organic components from positive matrix factorization of aerosol mass spectrometric data. Atmos. Chem. Phys. 9, 2891–2918.
Wang, J.F., Zhang, Q., Chen, M.D., Collier, S., Zhou, S., Ge, X.L., et al., 2017. First chemical characterization of refractory black carbon aerosols and associated coatings over the Tibetan Plateau (4730 m a.s.l). Environ. Sci. Technol. 51, 14072–14082.
Wang, Q., Shao, M., Zhang, Y., Wei, Y., Hu, M., Guo, S., 2009. Source apportionment of fine organic aerosols in Beijing. Atmos. Chem. Phys. 9, 8573–8585.
Wang, X., Williams, B.J., Wang, X., Tang, Y., Huang, Y., Kong, L., et al., 2013. Characterization of organic aerosol produced during pulverized coal combustion in a drop tube furnace. Atmos. Chem. Phys. 13, 10919–10932.
Wang, Y.H., Liu, Z.R., Zhang, J.K., Hu, B., Ji, D.S., Yu, Y.C., et al., 2015. Aerosol physicochemical properties and implications for visibility during an intense haze episode during winter in Beijing. Atmos. Chem. Phys. 15, 3205–3215.
Weber, R.J., Sullivan, A.P., Peltier, R.E., Russell, A., Yan, B., Zheng, M., et al., 2007. A study of secondary organic aerosol formation in the anthropogenic influenced southeastern United States. J. Geophys. Res.-Atmos. 112, D13302.
Wong, J.P.S., Lee, A.K.Y., Abbatt, J.P.D., 2015. Impacts of sulfate seed Acidity and water content on isoprene secondary organic aerosol formation. Environ. Sci. Technol. 49, 13215–13221.
Xiang, P., Zhou, X.M., Duan, J.C., Tan, J.H., He, K.B., Yuan, C., et al., 2017. Chemical characteristics of water-soluble organic compounds (WSOC) in $PM_{2.5}$ in Beijing, China: 2011-2012. Atmos. Res. 183, 104–112.
Xu, L., Guo, H.Y., Weber, R.J., Ng, N.L., 2017. Chemical characterization of water-soluble organic aerosol in contrasting rural and urban environments in the Southeastern United States. Environ. Sci. Technol. 51, 78–88.
Xu, J., Zhang, Q., Chen, M., Ge, X., Ren, J., Qin, D., 2014. Chemical composition, sources, and processes of urban aerosols during summertime in northwest China: insights from high-resolution aerosol mass spectrometry. Atmos. Chem. Phys. 14, 12593–12611.
Xu, Q.C., Wang, S.X., Jiang, J.K., Bhattarai, N., Li, X.X., Chang, X., et al., 2019. Nitrate dominates the chemical composition of $PM_{2.5}$ during haze event in Beijing, China. Sci. Total Environ. 689, 1293–1303.
Xu, W.Q., Sun, Y.L., Chen, C., Du, W., Han, T.T., Wang, Q.Q., et al., 2015b. Aerosol composition, oxidation properties, and sources in Beijing: results from the 2014 Asia-Pacific Economic Cooperation summit study. Atmos. Chem. Phys. 15, 13681–13698.
Xu, J.Z., Zhang, Q., Wang, Z.B., Yu, G.M., Ge, X.L., Qin, X., 2015a. Chemical composition and size distribution of summertime $PM_{2.5}$ at a high altitude remote location in the northeast of the Qinghai-Xizang (Tibet) Plateau: insights into aerosol sources and process in free troposphere. Atmos. Chem. Phys. 15, 5069–5081.
Yang, Y.R., Liu, X.G., Qu, Y., An, J.L., Jiang, R., Zhang, Y.H., et al., 2015. Characteristics and formation mechanism of continuous hazes in China: a case study during the autumn of 2014 in the North China Plain. Atmos. Chem. Phys. 15, 8165–8178.
Ye, Z.L., Liu, J.S., Gu, A.J., Feng, F.F., Liu, Y.H., Bi, C.L., et al., 2017. Chemical characterization of fine particulate matter in Changzhou, China, and source apportionment with offline aerosol mass spectrometry. Atmos. Chem. Phys. 17, 2573–2592.
Zhang, J.K., Sun, Y., Liu, Z.R., Ji, D.S., Hu, B., Liu, Q., et al., 2014. Characterization of submicron aerosols during a month of serious pollution in Beijing, 2013. Atmos. Chem. Phys. 14, 2887–2903.
Zhang, Q., Jimenez, J.L., Canagaratna, M.R., Ulbrich, I.M., Ng, N.L., Worsnop, D.R., et al., 2011. Understanding atmospheric organic aerosols via factor analysis of aerosol mass spectrometry: a review. Anal. Bioanal. Chem. 401, 3045–3067.
Zhang, R., Jing, J., Tao, J., Hsu, S.C., Wang, G., Cao, J., et al., 2013. Chemical characterization and source apportionment of $PM_{2.5}$ in Beijing: seasonal perspective. Atmos. Chem. Phys. 13, 7053–7074.
Zhang, Y.Y., Lang, J.L., Cheng, S.Y., Li, S.Y., Zhou, Y., Chen, D.S., et al., 2018a. Chemical composition and sources of PM_1 and $PM_{2.5}$ in Beijing in autumn. Sci. Total Environ. 630, 72–82.
Zhang, Y.L., El-Haddad, I., Huang, R.J., Ho, K.F., Cao, J.J., Han, Y.M., et al., 2018b. Large contribution of fossil fuel derived secondary organic carbon to water soluble organic aerosols in winter haze in China. Atmos. Chem. Phys. 18, 4005–4017.
Zhao, X.J., Zhao, P.S., Xu, J., Meng, W., Pu, W.W., Dong, F., et al., 2013. Analysis of a winter regional haze event and its formation mechanism in the North China Plain. Atmos. Chem. Phys. 13, 5685–5696.
Zheng, G.J., Duan, F.K., Su, H., Ma, Y.L., Cheng, Y., Zheng, B., et al., 2015. Exploring the severe winter haze in Beijing: the impact of synoptic weather, regional transport and heterogeneous reactions. Atmos. Chem. Phys. 15, 2969–2983.
Zheng, M., Salmon, L.G., Schauer, J.J., Zeng, L.M., Kiang, C.S., Zhang, Y.H., et al., 2005. Seasonal trends in $PM_{2.5}$ source contributions in Beijing, China. Atmos. Environ. 39, 3967–3976.
Zhou, W., Jiang, J.K., Duan, L., Hao, J.M., 2016. Evolution of submicron organic aerosols during a complete residential coal combustion process. Environ. Sci. Technol. 50, 7861–7869.
Zorn, S.R., Drewnick, F., Schott, M., Hoffmann, T., Borrmann, S., 2008. Characterization of the South Atlantic marine boundary layer aerosol using an aerodyne aerosol mass spectrometer. Atmos. Chem. Phys. 8, 4711–4728.